Journal of Power Sources 195 (2010) 3201–3206

Contents lists available at ScienceDirect

Journal of Power Sources

journal homepage: www.elsevier.com/locate/jpowsour

Passive water management at the cathode of a planar air-breathing proton exchange membrane fuel cell

T. Fabian[a,*], R. O'Hayre[b], S. Litster[a], F.B. Prinz[a], J.G. Santiago[a]

[a] Department of Mechanical Engineering, Stanford University, Stanford, CA 94305, USA
[b] Department of Metallurgical and Materials Engineering, Colorado School of Mines, Golden, CO 80401 USA

ARTICLE INFO

Article history:
Received 6 October 2009
Received in revised form 2 December 2009
Accepted 2 December 2009
Available online 14 December 2009

Keywords:
PEM fuel cells
Passive air-breathing fuel cell
Water management
Cathode flooding
Wicking media

ABSTRACT

Water management is a significant challenge in portable polymer electrolyte membrane (PEM) fuel cells and particularly in proton exchange membrane (PEM) fuel cells with air-breathing cathodes. Liquid water condensation and accumulation at the cathode surface is unavoidable in a passive design operated over a wide range of ambient and load conditions. Excessive flooding or dry out of the open cathode can lead to a dramatic reduction of fuel cell power. We report a water management design based on a hydrophilic and electrically conductive wick. A prototype air-breathing fuel cell with the proposed water management design successfully operated under severe flooding conditions, ambient temperature 10 °C and relative humidity of 80%, for up to 6 h with no observable cathode flooding or loss of performance.

1. Introduction

The demand for improved power solutions for portable applications has spurred significant research into miniature fuel cells. Traditional fuel cell systems are complex and bulky; often requiring many auxiliary components such as humidifiers, pumps, compressors, fans and heat sinks. These are in addition to the fuel container and the actual fuel cell. The challenge faced by designers of a miniature fuel cell aimed at replacing batteries in portable power applications is in downscaling and simplifying the existing fuel cell architectures, and at the same time matching the robustness, range of operating conditions and cost of batteries and outperforming their energy density [1].

Water management is a crucial part of any fuel cell system and can be particularly challenging to miniaturize. Most fuel cells for portable applications use polymer electrolyte membranes (PEM), such as Nafion™, as an electrolyte. To obtain high ionic conductivity, these membranes must be fully saturated with water [2–4]. For efficient operation, therefore, PEM-based fuel cells require water-balanced operation under all operating conditions. Insufficient water production leads to membrane and catalyst layer dry out, causing an increase in resistive and activation losses. On the other hand, excessive water production leads to condensation and flooding, which in turn causes an increase in mass transfer losses [5,6].

Many approaches have been developed for fuel cell water management: upstream reactant flow humidification [2,7], cathode water removal by positive cathode to anode gas pressure differential [8,9], water removal by super-stoichiometric flow [10,11] or transient purge [12,13], and water removal by the formation of a pressure gradient between a flow channel and a coolant channel through a porous bipolar plate [14]. For a detailed review see also [15]. Although these water management techniques differ in implementation, they all require bulky components such as humidifiers, blowers, compressors, and are largely unsuitable for miniature planar architectures.

Planar air-breathing polymer electrolyte fuel cells are attractive for the smallest portable power applications due to their simple construction and minimum balance of plant [16–23]. They are characterized by open-cathode architectures whereby delivery of oxygen from ambient air occurs by diffusion and natural convection (or small amounts of forced convection by local atmospheric or room conditions). As a consequence of the open-cathode construction, water-balanced operation is difficult to achieve over a wide range of operating conditions. None of the aforementioned techniques for water management can be applied in a planar open-cathode design due to the lack of control of the relative humidity and temperature of the ambient air as well as the absence of flow channels with pressure gradients for liquid water advection.

The specific architecture and requirements posed by air-breathing cells demand nontraditional water management

* Corresponding author at: Stanford University, Mechanical Engineering, Building 530, Room 226, Stanford, CA 94305, USA. Tel.: +1 650 723 7629; fax: +1 650 723 5034.
E-mail address: tfabian@gmail.com (T. Fabian).

0378-7753/$ – see front matter © 2009 Elsevier B.V. All rights reserved.
doi:10.1016/j.jpowsour.2009.12.030

approaches. Yao et al. [24] proposed a water management design at the cathode of a miniature air-breathing direct methanol fuel cell (DMFC) based on selective hydrophilic/hydrophobic cathode patterning, variation in cathode through-hole diameter, and gravity driven droplet flow. This architecture enables recirculation of product water but is strongly orientation dependent. In simultaneous work, we presented a demonstration of the use of patterned wicks for water management in air-breathing cathodes [25].

Water management with hydrophilic wicks or water-collecting layers has already been demonstrated in fuel cells. For example, Ge et al. [26,27] embedded polyvinyl alcohol (PVA) wicks into gas flow channels for water redistribution. However, internal wicks alone cannot prevent flooding since they have finite storage capacity. Furthermore, PVA wicks are non-conductive, require flow channel modifications, and obstruct current paths. As an alternative, Yi et al. [14] implemented a hydrophilic porous graphite plate to serve simultaneously as gas flow manifold and to remove excess water. Water flow from the cathode channels through the porous plate is accomplished by a positive pressure gradient between the cathode flow channels and coolant channels and/or anode flow channels located in the vicinity of the cathode flow channels. This approach simplifies the integration of the wicking structure and can eliminate flooding in a closed stack manifold, but cannot be directly implemented in an air-breathing cathode due to the lack of a closed cathode channel and the requirement for a compressor.

In this paper we report on an approximately scalable, orientation-independent, water management design for an open-air breathing cathode based on a hydrophilic and electrically conductive wick. The hydrophilic conductive wick is in direct contact with cathode gas diffusion layer (GDL) and serves as a water collector and distributor layer which hydraulically links the entire cathode surface. We then discuss the performance of this wicking strategy in the context of a simple cathode water balance model based on our earlier experimental observations [28] and modeling efforts [5], and propose modifications to our model to capture surface flooding effects.

2. Experimental methodology

In this section we present details of the experimental setup: design of the planar fuel cell, water collector layer, and the measurement protocol.

2.1. Fuel cell hardware

The experimental cell consists of several functional layers stacked on top of each other and held together with bolts. The outer dimensions of the system were 7 cm × 7 cm × 1 cm. The hydrogen feed chamber is a Delrin back-plate with two hydrogen distribution channels (each 5 mm wide, 5 mm deep, and 3 cm long). We use a printed circuit board (PCB)-based anode with 10 1.5 mm wide parallel flow channels spaced 1.5 mm apart. We use a self-humidifying, Nafion 112-based 5-layer membrane electrode assembly (MEA) (BCS Fuel Cells Inc., Bryan, TX) with 3 cm × 3 cm active area and 1 mg cm^{-2} catalyst loading on both sides. Silicone rubber gaskets placed between individual layers seal the anode compartment and provide for optimal MEA compression. The top layer of the cathode consists of a rigid printed circuit board (PCB) superstructure with 10 parallel ribs 1.5 mm wide with edges spaced by 1.5 mm. In our experiments we compare two cathode assemblies. Fig. 1a shows a schematic cross-section of the first cell assembly (showing only two neighboring cathode ribs), where the cathode current collector PCB superstructure is in direct contact with the cathode GDL. This is a traditional cathode current collector arrangement and serves to demonstrate the impact of cathode flooding. Fig. 1b shows

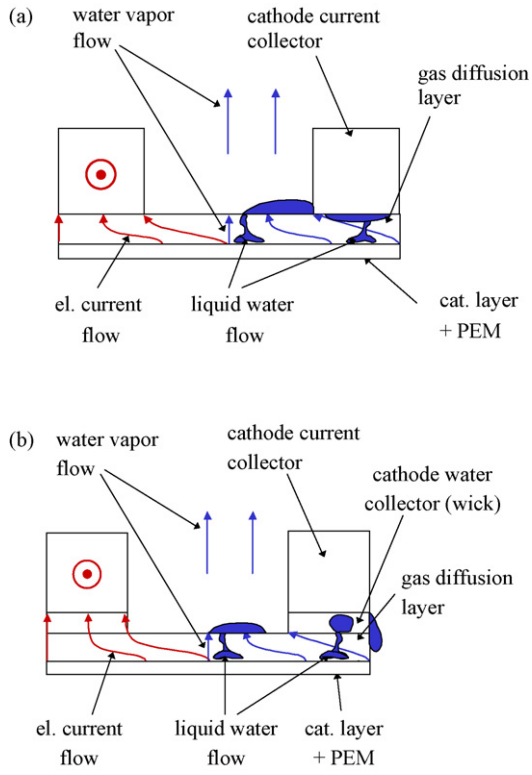

Fig. 1. Schematic cross-section views of an air-breathing cathode without (a) and with (b) a porous, hydrophilic, thermally and electrically conductive wick serving as an integrated water collector layer.

a schematic cross-section of the second cell assembly with water collector layer constructed of 1.5 mm thick porous graphite plate GDM 1.5-1000 (Sigracet, SGL Technologies, St. Marys, PA), embedded between the cathode GDL and cathode current collector. The porous graphite has a mean pore diameter of 38 mm, 60% porosity, and about 8 cm water rise height. Parallel through-slots identical with the channels of the cathode PCB superstructure are machined into the graphite plate for air access. The water collectors underneath the ribs are interconnected through water collector areas at the circumference of the cell. Exploded view of the cathode half of the single cell air-breathing fuel cell stack is shown in Fig. 2.

2.2. Experimental setup

We use an experimental setup consisting of an environmental chamber, DC load, and a potentiostat. Detailed description of the

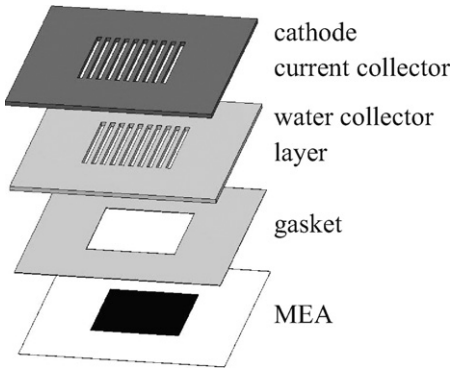

Fig. 2. Exploded view of the air-breathing fuel cell cathode comprising 3 cm × 3 cm active area MEA, gasket, in plane water collector, and cathode current collector. For simplicity tension bolts and assembly holes are not shown.

experimental setup can be found in [28]. The air-breathing cell ran on dry hydrogen with a dead-ended anode inside of the environmental chamber. A DC load attached to the fuel cell controlled by a LabView script on a PC set the current of the cell.

2.3. Measurement procedure

We have characterized the performance of the air-breathing fuel cell with and without the water collector layer by a set of galvanostatic measurements. During the measurements the current was set to a constant value and the cell voltage as well as the cell surface temperature were recorded until either the cell voltage collapsed or a steady state was attained. The temperature of the cell was recorded with a fine gauge unsheathed K-type thermocouple (Omega) on the top surface of the cathode current collector rib in the geometric center of the open-cathode area. The overall duration of each galvanostatic measurement was up to 6 h. Separate galvanostatic measurements were made at current densities of 100, 200, 300, 400, 500, and 600 mA cm^{-2}, respectively. The fuel cell was always operated under heavy flooding conditions: dead-ended anode gas flow, open-cathode area horizontal and facing upwards, natural convection above the cathode, and ambient conditions set to 10 °C and 80% relative humidity.

Before each measurement, the fuel cell cathode and anode were purged with compressed air and any liquid water accumulated on or in the cell was removed. Then, the anode compartment was purged with hydrogen, the anode outlet was sealed, and the anode flow meter was checked for indications of a leak. Typical open cell voltage hydrogen flow rates were about 0.5 sccm. After the anode purge the cell was first connected to both the load and the potentiostat and then it was placed inside the environmental chamber. The cell's temperature and membrane humidity were allowed to equilibrate for about 10 min prior to each measurement.

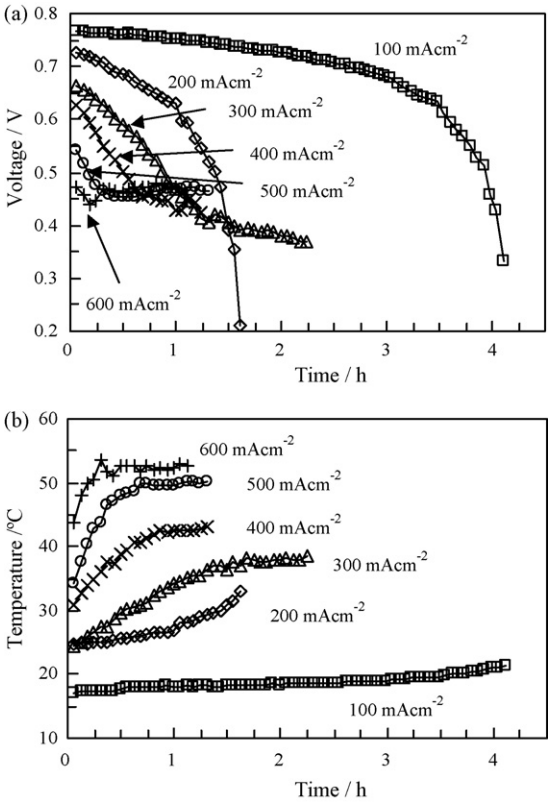

Fig. 3. Characteristic measurements of cell potential (a) and cathode temperature (b) as a function of time for current densities ranging from 100 to 600 mA cm^{-2} for a control case, air-breathing cathode without an embedded water collector layer. The ambient conditions were 10 °C and 80% relative humidity.

3. Results

In these experiments we characterized the long-term stability of an air-breathing fuel cell with and without cathode water collector while operated under severe flooding conditions. Both cell potential and cathode surface temperature were recorded.

3.1. Control case of a cathode without water management

Fig. 3a shows typical measurement of the cell potential during galvanostatic operation as a function of time for current densities ranging from 100 to 600 mA cm^{-2} for the control cathode without the water collector. The cell voltage varied significantly over time with two distinct time constants. In the first few minutes (<5 min) the cell voltage quickly rose and reached a maximum value; during this period the cathode was free of any liquid water. In the second interval, associated with a gradual buildup of liquid water on the cathode surface, the cell voltage gradually decreased and the rate of decrease accelerated with time. At current density settings of 100 and 200 mA cm^{-2}, the cathode flooding led to complete surface blockage and the cell voltage collapsed to zero without achieving a steady state working condition. On the other hand at load currents at and above 300 mA cm^{-2}, the cathode flooding did not completely block the surface. Instead, both the cell voltage and the fraction of cathode water surface coverage eventually stabilized. For increasing values of current density, this stability point was characterized by decreasingly smaller fraction of equilibrium water surface coverage. At a current density of 600 mA cm^{-2} no liquid water was observed at the cathode surface. Furthermore, the equilibrium condition was achieved more rapidly with increasing current density. The larger the load current, the faster the buildup of water on the cathode surface, and the faster the cell either completely flooded or reached a stable equilibrium.

Fig. 3b shows the corresponding cathode surface temperatures as a function of time for current densities between 100 and 600 mA cm^{-2}. These cathode temperature time series show dynamics similar to the cell voltage. In cases that lead to a steady state, the cell temperature rose quickly to an initial value in less than ~5 min (not shown here), then gradually increased (during which we observed liquid buildup at the surface), and eventually saturated at a stable value. In cases with no apparent steady state, the initial temperature rise was followed by a slow but accelerating temperature rise without a stable endpoint (e.g., the 100 and 200 mA cm^{-2} cases).

3.2. Cathode with water collector layer

In a second set of experiments we investigated the long-term stability of an air-breathing fuel cell with the integrated water collector layer. The water collector layer used in these experiments extended to the cell circumference where it formed a 2 cm wide frame region, thus providing a large water buffer capacity. The cell was operated under the same conditions as in the experiments associated with Fig. 2. For the durations explored here, the wick absorbed and drained all the water condensed in the cathode channels without achieving full saturation of the frame region in the periphery. However, even under the limit of full wick saturation, we observed that water preferentially escapes via gravity (dripping) from the wick at the cell circumference (at or near the lowest point) rather than flooding the cathode channels.

Characteristics measurements quantifying fuel cell potential and cathode surface temperature for a cathode with water collec-

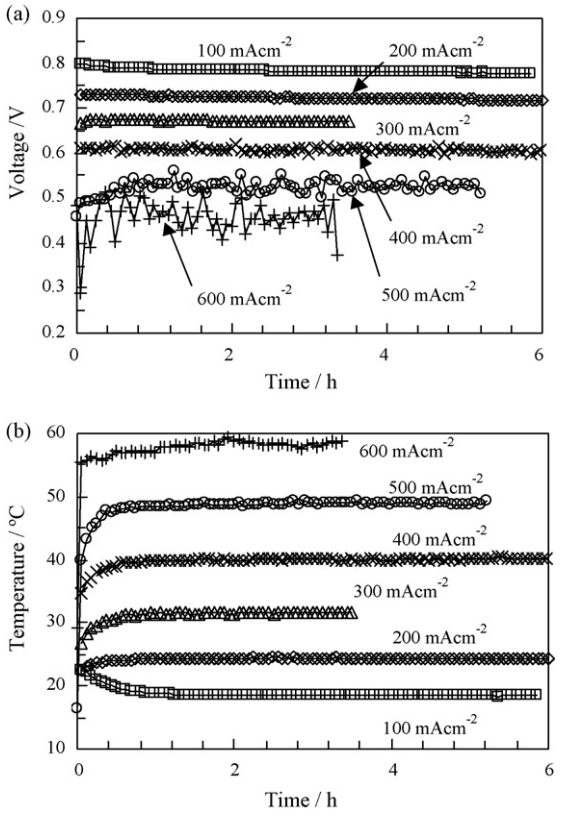

Fig. 4. Measurements of cell potential (a) and cathode temperature (b) as a function of time for current densities ranging from 100 to 600 mA cm^{-2} for an air-breathing cathode with an embedded water collector layer. The ambient conditions were 10 °C and 80% relative humidity.

tor as a function of time for current densities ranging from 100 to 600 mA cm^{-2} are shown in Fig. 4a and b, respectively. Similar to the control experiments without the water collector layer, the cell voltage and cathode temperature initially rose quickly (<5 min) after the load current was established. However, for this arrangement, the fuel cell potential and cathode temperature remained relatively stable thereafter for the entire duration of the experiment (6 h). In contrast to the control case, the cell voltages were stable at all measured current settings. Also, the setup with the wick exhibited slightly lower temperatures than the steady state values achieved by the control case.

4. Discussion

In this section we briefly describe a simple water flux balance model at the cathode of an air-breathing PEM fuel cell, and then use it to help interpret the experimental results.

4.1. Steady state water flux balance at the cathode of an air-breathing fuel cell (control case of no water collector layer)

The water flux balance at the open-air cathode of a passive air-breathing fuel cell is controlled by mutually coupled heat and mass transfer processes [5]. Under the simplifying assumption of a dead-ended anode, and zero hydraulic pressure between anode and cathode (and zero anode water flux) and under steady state conditions (no water accumulation), the water flux generated at the cathode catalyst must equal the convective flux away from the cathode. In the absence of gravity driven liquid flow (cathode horizontal facing upwards) the convective water flux at the cathode occurs only in vapor form and the water flux balance can be

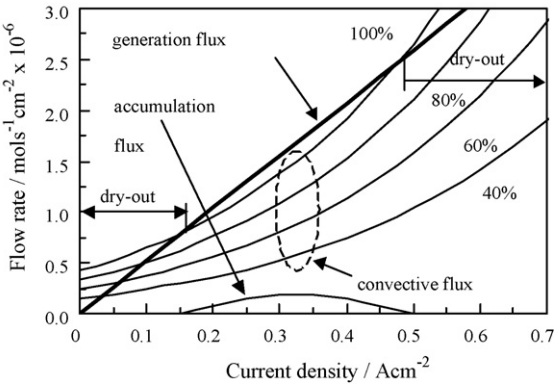

Fig. 5. Plot of predicted generated water flux and cathode vapor flux from Eq. (1) as a function of current density for different values of cathode-surface relative humidity, RH_{gdl}. The parameters used to generate the plots were based on experimental observations of [28] and [6] and the following selections: convective mass transfer coefficient $h = 0.35$ cm s^{-1}, ambient temperature $T_{amb} = 26$ °C, and ambient relative humidity $RH_{amb} = 10\%$. The cathode surface temperature was increased by 7.2 °C for each 100 mA cm^{-2}. The generation flux (the thicker straight line) is the molar flux of water generated by the fuel cell reaction. The convective (water vapor) flux lines are shown for surface relative humidity ranging from 40 to 100% as per Eq. (1). The accumulation flux curve is the generation flux minus convective flux at surface humidity of 100% when this difference is positive and zero otherwise. The "dry out" labels shown apply only to the convective flux case of 100% relative humidity at the surface.

expressed as [5]:

$$\frac{j}{2F} = \frac{h}{R}\left(RH_{gdl}\frac{p_{sat}(T_{gdl})}{T_{gdl}} - RH_{amb}\frac{p_{sat}(T_{amb})}{T_{amb}}\right) \quad (1)$$

where j is the current density, F the Faraday constant, T_{gdl} the surface temperature of the cathode, RH_{gdl} the relative humidity at the cathode surface, h the natural convection mass transfer coefficient, R the universal gas constant, p_{sat} the saturated water vapor pressure, T_{amb} ambient temperature, and RH_{amb} is the ambient relative humidity.

The cathode convective water flux is driven by the difference in water vapor concentration between the cathode surface and ambient. For a given ambient relative humidity and temperature, the saturated water vapor pressure at the cathode surface therefore limits the maximum cathode water flux. In general, the cathode surface temperature and current density are coupled due to self-heating. For a qualitative understanding of the water flux balance in Eq. (1) as a function of current density we will assume a linear dependence between cathode surface temperature and current density, as suggested by many transient polarization measurements in [28]. This is a simplifying but useful assumption based on experimental data and we will revisit it later in light of our experimental observations. The convective water vapor transfer presents a bottleneck in water transport; and flooding occurs when the cathode water generation rate exceeds the maximum cathode vapor flux.

Fig. 5 shows an example plot of the predicted steady state water flux balance in Eq. (1) based on a linear dependence between cell current and cathode surface temperature. The parameters used to generate these curves were selected to show cell operation with distinct regions of flooding and dry out, $RH_{amb} = 10\%$, $T_{amb} = 26$ °C, and a typical temperature change per current of $dT/dj = 72$ °C A^{-1} cm^{-2}, see also [28]. The generated water flux versus current density is linear with slope and equal to $1/2F$. On the other hand the convective flux increases exponentially with current density due to the coupling between current density and cathode surface temperature (and the exponential dependence of vapor pressure on temperature). Shown are data for four values of cathode surface relative humidity RH_{gdl}: 40%, 60%, 80%, and 100%.

For a given current density, if the water generation flux exceeds the convective flux, then surface humidity increases until the convective flux equals generation flux or surface humidity reaches 100%. When the cathode surface humidity reaches 100%, if the generation flux still exceeds convective flux, then water vapor cannot carry additional water and liquid water builds up on the surface. If at 100% surface humidity the generation flux is less than the convective flux, then we can expect eventual dry out.

In Fig. 5 the line for convective flux with 100% surface relative humidity (the maximum convective flux) intersects with the water generation line twice, suggesting that there are at least three distinct regions associated with net water accumulation. At current densities below the first and above the second intersection, all of the generated water is removed from the cathode surface and the membrane is less than 100% humidified. At the intersection points the membrane is fully saturated and the generated water flux equals the maximum convective water flux. These intersection points represent ideal operating conditions since the membrane is fully humidified (low ohmic resistance) without cathode flooding. (We note that the current analysis does not tell us if these operating points are expected to be stable or unstable.) Between the two intersection points is a flooding regime where the generated water flux exceeds the maximum cathode convective flux and liquid water accumulates at the cathode surface. Here, the assumption of linear temperature increase with current density suggests that a steady state water balance according to Eq. (1) cannot be established and the cell catastrophically floods. Despite its limiting assumptions, the general behavior predicted by this simple model is consistent with transient polarization scans [28].

Our experiments corroborate many of the trends predicted by the simple model above. For example, for the control case without the water collector layer, cell performance often quickly degraded when operated at intermediate current densities associated with flooding conditions. We observed liquid water on the cathode surface at current densities from 100 to 500 mA cm^{-2}, indicating flooded performance. Interestingly, despite the presence of liquid water, steady state operation was achieved at current densities from 300 to 500 mA cm^{-2} (see Fig. 3). This behavior is not predicted by the model. As we discuss below, we believe this implies that the assumption of linear dependence of cathode temperature on current density is not valid at high current density.

Comparison of the simple model and the experimental data suggests that cathode temperature may have a non-linear dependence on current density. The experimental data for the control case (no wick) suggests that cell operation may be stable at relatively high current densities (see 500 and 600 mA cm^{-2} traces in Fig. 2). We hypothesize that cell voltage stabilization in partially flooded, high current density conditions is caused by a positive feedback: increasing cathode surface water coverage causes increased self heating, leading to faster surface evaporation. The cathode temperature is apparently coupled to the cell potential: the lower the cell voltage, then the higher the cell temperature (at fixed current density).

The cathode temporal responses are consistent with our hypothesis. Similarly to the cell potential response, the cathode temperature temporal response shows two characteristic time constants. During first few minutes the cathode surface temperature rises from ambient to an intermediate value. This time constant is likely determined by the thermal mass of the fuel cell assembly (this brief initial transient is not shown in the plot). Then, as water gradually condenses on the cathode surface and blocks air access to the cathode, the cell voltage gradually decreases, lowering the fuel cell efficiency, increasing the heat losses, and consequently further increasing the surface temperature and evaporation rate.

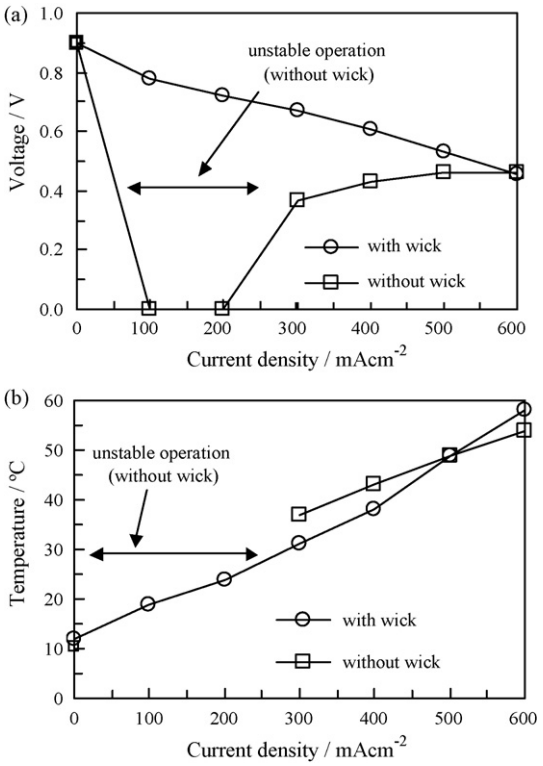

Fig. 6. Plots of steady state polarization curves (a) and cathode temperature profiles (b) for a planar fuel cell with an air-breathing cathode with and without water collector layer. For the potential measurements of the no wick control case, we show the unstable, degrading cell behavior as zero potential. We do not plot the cell temperature for the no wick cases for which we observed no steady state working behavior.

4.2. Impact of water collector on cathode flooding

The system with the water collector showed only small water droplets on the cathode surface. These typically grew slightly and eventually contacted and were pulled into the wick. The system was stable for all current settings. The water collector hydraulically links the entire area of the cathode, while allowing sufficient supply of oxygen from atmospheric air. Oxygen access was achieved by patterning the water collector layer with cutouts significantly larger than the pore size of the water collector. Since the wick was a single piece, it provides a hydraulic link between any two areas of the water collector. Consequently, when in contact with liquid water, the water likely first saturated the wick and filled small pore volumes (which have the highest capillary pressure). For simplicity the water collector in Fig. 1b employs a cutout pattern identical to the openings in the cathode current collector. We performed limited experiments with other wick shapes (not shown here), and concluded that collector layers with shapes independent of the cathode current collector pattern are also feasible.

The flux of water from the GDL surface into the water collector is driven by two different mechanisms. Initially, when the wick is entirely or partially dry, capillary forces drive the liquid into the water collector. However, once the wick is fully saturated the capillary-pressure-driven flux stops. Beyond this point liquid water is driven out of the water collector by the pressure gradients created by water evaporation from the collector surface and gravity.

Data demonstrating the effect of water removal from the cathode is summarized in Fig. 6. Fig. 6a presents the steady state IV plots for the control case and the cathode with the water collector layer. The value of the steady state cell potential (obtained from Figs. 3a or 4a) is plotted for each current density. In cases where

fuel cell performance degraded due to flooding without reaching a steady state we plot values of zero potential.

Both control and wick configurations are stable at open cell voltage, showing accumulation due to hydrogen crossover is negligible. The control case (no wick) operation was not stable at intermediate current densities of 100 and 200 mA cm^{-2} where steady state cell voltage collapses due to flooding. The critical current density above which the fuel cell floods was apparently smaller than 100 mA cm^{-2}. At and above 300 mA cm^{-2} the control case shows a stable steady state cell voltage. However, the cell potential is reduced by as much as 0.35 V (due to flooding) compared to the cell with the water collector. As the cell current is increased, the difference between the steady state cell voltages with and without the water collector decreased. Theoretically, this difference should approach negligible values at and above the hypothesized third critical current density above which the control cell enters the dry out regime. Above this critical current density both cathode configurations should behave similarly and eventually reach dry out.

Fig. 6b shows the steady state cathode temperatures for the control case and the cathode with the water collector layer obtained from Figs. 3b or 4b. We do not plot temperature values in cases where steady state operation was not achieved. The temperature profile for the cell with water collector is approximately linear with current density for most of the current densities. The control case (no water collector) has a higher steady state temperature (maximum difference of about 6 °C) than the case without wick; and this is consistent with our hypothesis that there is a positive feedback controlling partial flooding.

5. Conclusions

Galvanostatic measurements suggest that flooding in a control case, air-breathing cathode (no wick), can lead either to a catastrophic flooding or to a partially flooded surface accompanied by decreased cell potential and the associated fuel cell energy conversion efficiency.

To address the severe effects of flooding, we introduced a thin electrically conductive water collector (a patterned wick) layer between the current collector and the cathode surface. The water collector initially absorbs and redistributes any liquid water across the entire cathode and eventually allows the liquid to escape outside of the cathode area without obstructing the cathode oxygen supply. Our results show that the water collector layer eliminates the effects of cathode flooding and allows efficient cell operation within a wide operational window, at a small cost of increased cathode complexity.

References

[1] L.H. Maynard, P.J. Meyers, J. Vac. Sci. Technol. B 20 (2002) 1287–1297.
[2] T.E. Springer, T.A. Zawodzinski, S. Gottesfeld, J. Electrochem. Soc. 138 (1991) 2334–2342.
[3] J. Fimrite, B. Carnes, H. Struchtrup, N. Djilali, J. Electrochem. Soc. 152 (2005) A1815–A1823.
[4] Y. Sone, P. Ekdunge, D. Simonsson, J. Electrochem. Soc. 143 (1996) 1254–1259.
[5] R. O'Hayre, T. Fabian, S. Litster, J.G. Santiago, F.B. Prinz, J. Power Sources 167 (2007) 118–129.
[6] T. Fabian, R. O'Hayre, F.B. Prinz, J.G. Santiago, J. Electrochem. Soc. 154 (2007) B910–B918.
[7] T.E. Springer, T.A. Zawodzinski, M.S. Wilson, S. Gottesfeld, J. Electrochem. Soc. 143 (1996) 587–599.
[8] D.P. Wilkinson, H.H. Voss, K. Prater, J. Power Sources 49 (1994) 117–127.
[9] D.M. Bernardi, M.W. Verbrugge, J. Electrochem. Soc. 139 (1992) 2477–2491.
[10] U. Pasaogullari, C.Y. Wang, J. Electrochem. Soc. 152 (2005) A380–A390.
[11] K. Tuber, D. Pocza, C. Hebling, J. Power Sources 124 (2003) 403–414.
[12] H.H. Voss, D.P. Wilkinson, P.G. Pickup, M.C. Johnson, V. Basura, Electrochim. Acta 40 (1995) 321–328.
[13] E. Antolini, R.R. Passos, E.A. Ticianelli, J. Appl. Electrochem. 32 (2002) 383–388.
[14] J.S. Yi, J.D.L. Yang, C. King, AIChE J. 50 (2004) 2594–2603.
[15] C.R. Buie, J.D. Posner, T. Fabian, C.A. Suk-Won, D. Kim, F.B. Prinz, J.K. Eaton, J.G. Santiago, J. Power Sources 161 (2006) 191–202.
[16] T. Hottinen, I. Himanen, P. Lund, J. Power Sources 138 (2004) 205–210.
[17] C. Ziegler, A. Schmitz, M. Tranitz, E. Fontes, J.O. Schumacher, J. Electrochem. Soc. 151 (2004) A2028–A2041.
[18] A. Schmitz, M. Tranitz, S. Wagner, R. Hahn, C. Hebling, J. Power Sources 118 (2003) 162–171.
[19] T. Hottinen, M. Mikkola, P. Lund, J. Power Sources 129 (2004) 68–72.
[20] F. Jaouen, S. Haasl, W. Van Der Wijngaart, A. Lundblad, G. Lindbergh, G. Stemme, J. Power Sources 144 (2005) 113–121.
[21] S. Ha, B. Adams, R.I. Masel, J. Power Sources 128 (2004) 119–124.
[22] J.P. Meyers, H.L. Maynard, J. Power Sources 109 (2002) 76–88.
[23] D. Chu, R. Jiang, J. Power Sources 83 (1999) 128–133.
[24] S.C. Yao, X. Tang, C.C. Hsieh, Y. Alyousef, M. Vladimer, G.K. Fedder, C.H. Amon, Energy 31 (2006) 636–649.
[25] T. Fabian, R. O'Hayre, S. Litster, F.B. Prinz, J.G. Santiago, 210th ECS Meeting, in: T. Fuller, C. Bock, S. Cleghorn, H. Gasteiger, T. Jarvi, M. Mathias, T. Murthy (Eds.), Proton Exchange Membrane Fuel Cells 6, Cancun, Mexico, 2006, pp. 949–960.
[26] S.H. Ge, X.G. Li, I.M. Hsing, J. Electrochem. Soc. 151 (2004) B523–B528.
[27] S.H. Ge, X.G. Li, I.M. Hsing, Electrochim. Acta 50 (2005) 1909–1916.
[28] T. Fabian, J.D. Posner, R. O'Hayre, S.W. Cha, J.K. Eaton, F.B. Prinz, J.G. Santiago, J. Power Sources 161 (2006) 168–182.